Magnetic Field Alignment of Ordered Silicate-Surfactant Composites and Mesoporous Silica

Sarah H. Tolbert,* Ali Firouzi, Galen D. Stucky,† Bradley F. Chmelka†

Macroscopic orientational ordering of the pores of condensed hexagonal mesostructured silica (MCM-41) was achieved through alignment of an unpolymerized, hexagonal, lyotropic silicate-surfactant liquid crystal in a high magnetic field. This alignment was preserved after polymerization of the silicate species by acid treatment. Subsequent calcination to remove the surfactant yielded a mesoporous silica solid that retained both macroscopic pore alignment and mesoscale periodicity. Potential applications of such liquid crystal processing strategies range from the formation of anisotropic silica-based bulk ceramics to the production of oriented mesoporous thin films for chemical sensors, separations, catalysis, or host-guest applications.

The recent discovery (*1*) that inorganic silicate and organic surfactant precursors can self-organize (*2*) to form ordered materials with nanometer-scale periodicities has created exciting avenues for the synthesis of nanostructured materials. Ordered inorganic-surfactant composites have been made with a wide variety of transition metal (*3*, *4*) and main group oxides and phosphates (*5*, *6*, *7*, *8*) as well as metal chalcogenides (*9*). These composites have been shown to consist of aggregates of assembled surfactant molecules that interact covalently (*3*, *8*, *10*) or electrostatically (*1*, *6*, *8*) with an inorganic framework. For densely cross-linked inorganic mesostructures, it is frequently possible to remove the organic surfactant from the inorganic-surfactant composite by calcination or ion exchange to produce an ordered, mesoporous inorganic material with uniform pore sizes ranging from 20 to over 100 Å in diameter (*1*).

Many uses have been proposed for these mesoporous materials (*11*, *12*), most notably catalysis, separations, and chemical sensing of molecules that are too large for processing with crystalline zeolite molecular sieves, which generally have smaller (2 to 15 Å) micropores. Mesoporous solids may also be used as host matrices for optically (*13*, *14*) or electrically active (*15*) species. Many of these applications, however, are hindered by the fact that many mesoporous solids have to date been produced only as powders (*16*, *17*) with small domain sizes (≈1 μm) that have no orientational alignment of the pores over macroscopic length scales. Progress in orienting these materials has been made by growing thin films of mesoporous silicates at surfaces or interfaces (*18*–*21*), but the interface generally determines the alignment of the pores and frequently produces pores with orientations that are not desirable for the envisioned applications (*18*, *19*). In particular, the synthesis of mesoporous *p6mm* hexagonal (MCM-41) films with pores that are perpendicular to the plane of the film is a desirable goal (*16*).

The formation of silica mesophase solids under basic conditions (*1*) has been shown to proceed by the cooperative organization of solution-phase silicate and surfactant species coupled with inorganic polymerization (*22*). Under the appropriate conditions, however, mesophase self-assembly can be decoupled from inorganic polymerization to form silicate-surfactant liquid crystals in which the inorganic components remain as unpolymerized, oligomeric silicate anions (*2*, *23*). Recently, we have shown that it is possible to macroscopically orient such silicate-surfactant liquid crystals using an applied magnetic field (*24*). Deuterium (^{2}H) nuclear magnetic resonance (NMR) measurements indicate that the silicate-surfactant liquid crystals align on the basis of the collective diamagnetic susceptibilities of the molecular components of the material. Appreciable control over the alignment direction for both hexagonal (*p6mm*) and lamellar morphologies can be achieved by tuning the composition of the silicate-surfactant liquid crystal phase, especially the nature of the amphiphilic or organic cosolvent species (*24*).

Here, we show that it is possible to retain long-range alignment of hexagonal (*p6mm*) silicate-surfactant mesophases even after the inorganic component of the liquid crystal is polymerized by acidic or acidic-thermal treatment. Furthermore, the organic components of the polymerized composite can be removed by calcination without disruption of the macroscopic orientational order of the initial magnetic field–aligned material. The resulting bulk hexagonal mesoporous solid (MCM-41) exhibits long-range orientational ordering of the pores, which are aligned on average along the direction of the applied magnetic field. The uniaxial pore system created in this way holds promise for applications in a variety of systems in which uniaxial diffusion or orientational ordering of guest molecules is desired.

We prepared hexagonal silicate-surfactant liquid crystals by mixing a 7 to 12 weight % aqueous solution of the cationic surfactant cetyltrimethylammonium bromide (CTAB) and an aqueous alkaline silicate solution at room temperature to yield the overall molar ratio 1.0 SiO_2:0.31 CTAB:0.82 $(CH_3)_4N^+OH^-$:130 H_2O:14 CH_3OH (*24*). On mixing, the sample immediately phase-separated into a viscous silicate-surfactant–rich liquid crystalline phase and an aqueous-rich phase. Liquid crystal morphologies were characterized with ^{2}H NMR spectroscopy, x-ray scattering, and polarized optical microscopy (*23*). We oriented the silicate-surfactant liquid crystals in an 11.7-T magnetic field by heating the samples above their respective anisotropic-to-isotropic phase transition temperatures (50° to 90°C, depending on the composition), followed by slow cooling (≈5°C per hour in 3° to 5° steps) in the magnetic field. In situ ^{2}H NMR measurements were performed with α-deuterated CTAB to follow both liquid crystal phase behavior and the degree of alignment (Fig. 1) (*25*).

A series of ^{2}H NMR spectra of hexagonal silicate-surfactant liquid crystals are shown in Fig. 1. A powder pattern from an unaligned sample (12.9-kHz quadrupolar splitting), which is characteristic of a random distribution of hexagonal phase director orientations in three dimensions, is shown in Fig. 1A. After the sample was heated above its anisotropic-to-isotropic phase transition temperature (Fig. 1B) and cooled in the presence of the 11.7-T magnetic field, signal intensity was concentrated in the shoulder regions of the original powder spectrum [splitting = 26.5 kHz (Fig. 1C)]. This intensity distribution corresponds to alignment of the hexagonal phase directors in certain preferred orientations (*24*). Simulations (Fig. 1D) show that the spectrum in Fig. 1C can be reproduced from

S. H. Tolbert, Department of Chemistry, University of California, Santa Barbara, CA 93106, USA.
A. Firouzi and B. F. Chmelka, Department of Chemical Engineering, University of California, Santa Barbara, CA 93106, USA.
G. D. Stucky, Department of Chemistry and Materials Department, University of California, Santa Barbara, CA 93106, USA.
*Permanent address: Department of Chemistry and Biochemistry, University of California, Los Angeles, CA 90095–1569, USA.
†To whom correspondence should be addressed.

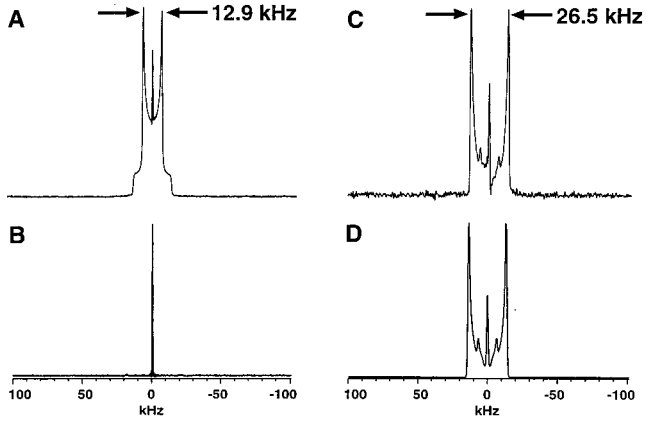

Fig. 1. In situ ^{2}H NMR spectra (**A** to **C**) and simulation (**D**) of a two-phase silicate-surfactant liquid crystal sample at pH = 12.5 made with α-deuterated CTAB showing different stages of the thermal and magnetic field alignment process. (A) Powder pattern at 25°C, corresponding to an initially unaligned hexagonal liquid crystal with a random distribution of domain directors. (B) Isotropic spectrum of a silicate-surfactant mesophase at 90°C, above the anisotropic-to-isotropic transition temperature of the liquid crystalline phase. The single peak indicates rapid, isotropic motion of the surfactant molecules corresponding to a loss of hexagonal order. (C) After slow cooling from 90° to 25°C in the presence of an 11.7-T magnetic field, the hexagonal liquid crystal phase is restored. The altered intensity distribution in the spectrum compared with that observed in (A) indicates appreciable alignment of the liquid crystalline domains within the sample. (D) Simulated ^{2}H NMR spectrum generated assuming 80% of the CTA^+ molecules are in hexagonal domains whose directors are oriented on average parallel to the applied field with a FWHM distribution of 55° ± 5°, 15% of the CTA^+ molecules are in randomly oriented hexagonal domains and 5% are rapidly mobile in the aqueous-rich phase.

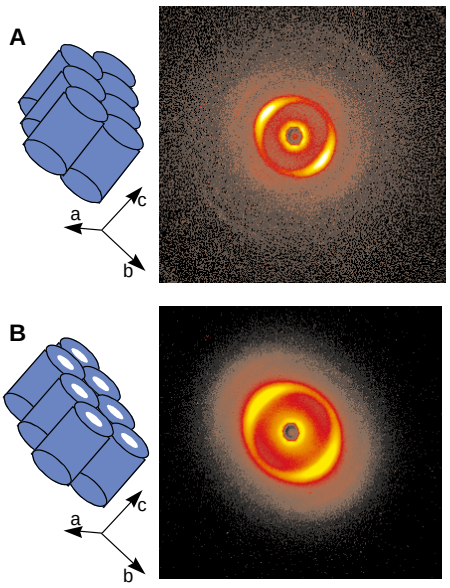

Fig. 2. Two-dimensional XRD data acquired from (**A**) a polymerized hexagonal silica-surfactant composite (prepared with method 1) and (**B**) calcined hexagonal mesoporous silica, both derived from the aligned liquid crystal intermediate of Fig. 1C. The nonuniform distribution of scattering intensity within the patterns indicates that the samples are oriented, as shown in the accompanying schematic diagrams, and that the materials have mesoscopic hexagonal periodicity. Scattering along a line from the upper left to the lower right corners of the images arises from the oriented composite. Scattering along an axis perpendicular to this in (A) results from a small amount of monoclinic crystalline CTAB (*39*). Small variations in the alignment axes in (A) and (B) are due to differences in sample position in the diffractometer and do not reflect a difference in pore orientation. In these images, 2θ is defined as the angular distance from the center point, and χ is defined as the angular extent of the scattering intensity around the rings (arcs in this case). The data in Figs. 3 and 4 were generated by integration of these 2D patterns around χ and radially in 2θ, respectively.

a model in which 80% of the cetyltrimethylammonium ions (CTA^+) reside in hexagonal phase domains whose uniaxial directors are oriented on average parallel to the applied magnetic field with a Gaussian distribution of 55 ± 5° full width at half maximum (FWHM) about the mean direction (*26*).

The high viscoelasticity of the oriented silicate-surfactant liquid crystals at room temperature allows them to be removed from the magnetic field for extended periods of time (several months) without loss of orientational order. Moreover, the field-induced alignment can be preserved during subsequent polymerization of the silicate component to form a mesostructured composite solid with a rigid silica framework that retains the orientational order of the precursor liquid crystal. Polymerization of the silicate species was induced by two different techniques. In the first method (which was used in the majority of experiments in this study), the aqueous-rich phase was separated from the silicate-surfactant–rich phase, and the latter was exposed to concentrated HCl vapor in a closed container for 1 to 3 days at room temperature (*27*). After removal from the acid vapor, samples were dried under mild vacuum to produce free-standing solid monoliths with dimensions on the order of 1 cm by 0.5 cm by 0.3 cm. In the second method, aqueous HBr was added to the two-phase mixture until the pH of the aqueous phase was between 11.4 and 11.6. This solution was kept at 45°C for 1 to 7 days; the aqueous phase was then decanted, and the sample was dried under mild vacuum at room temperature. Further thermal treatment in water at 100°C could be used to increase the extent of polymerization of the silica framework and improve the mesoscopic order of the product after calcination. The first method produced samples with better macroscopic alignment (that is, a larger fraction of oriented material), whereas the second method resulted in samples with higher mesoscopic order, but poorer macroscopic alignment.

Because of the loss of lateral surfactant mobility in the polymerized material, ^{2}H NMR cannot provide information about the structure or orientation of the acid-treated composites. The degree of orientational order in the polymerized composites (and also the calcined mesoporous solids, see below) was thus determined by two-dimensional (2D) x-ray diffraction (XRD) (Fig. 2) with a Siemens SMART charge-coupled device system equipped with Mo K-α radiation and modified for small-angle scattering down to 90 Å. Two-dimensional XRD can distinguish between different morphologies and also quantify material anisotropy. After polymerization by means of HCl vapor (method 1) of the same silicate-surfactant liquid crystal examined in Fig. 1 and subsequent drying of the composite, 2D XRD patterns (Fig. 2A) were obtained on single 2-mm pieces of the as-synthesized composite. These 2-mm pieces were cut from the larger 1 cm by 0.5 cm by 0.3 cm mass of oriented material and held in quartz capillaries. The image in Fig. 2A shows pairs of semicircular arcs at various distances from the center point; the more intense arcs, centered on a line from the upper left to the lower right of the image, correspond to the oriented hexagonal silicate-surfactant composite.

The diffraction patterns in Fig. 2 can be integrated in various ways to quantify the morphology and degree of alignment in the polymerized bulk silicate-surfactant composite. Powder XRD patterns [intensity versus 2θ (Fig. 3)] were obtained from 30° integrations around the radial χ direction and used to quantify the anisotropy of the sample. Integrations centered on the most intense regions of the diffraction pattern (Fig. 3, solid lines) correspond to the oriented fraction of the silica-surfactant composite. This aligned polymerized composite displays three diffraction peaks (Fig. 3A, solid line) that can be indexed to the hexagonal phase MCM-41(*1*). The second two of these peaks [(110) and (200)] are assignable but not well resolved. The dashed lines correspond to the radially uniform scattering intensity from a randomly oriented frac-

tion of the composite. The large difference between the solid and dashed integrations in Fig. 3A reflects the pronounced anisotropy of the polymerized silica-surfactant composite. Some scattering intensity corresponding to the hexagonal (100) diffraction peak can, however, be seen in the dashed integration in Fig. 3A; from these data, it can be estimated that about 78% of the sample is oriented (*28*). These results establish that the polymerized composite material has a hexagonal (*p6mm*) MCM-41 structure and that the *c* axes in the majority of the sample have a common uniaxial orientation; a distribution of orientations exist in the orthogonal *a*-*b* plane.

The degree of orientational order can be further quantified by integrating over the width of the $(100)_{hex}$ diffraction peak and plotting the result versus the radial angle χ (Fig. 4A). The results show a Gaussian distribution of orientations with a FWHM of 49°. Both the distribution and the overall fraction of oriented hexagonal material, as determined by XRD data, are in good agreement with the results obtained from ^2H NMR on the aligned liquid crystalline precursor (Fig. 1C), indicating that long-range orientational ordering of the mesophase domains was not disrupted by polymerization of the silicate oligomers into an extended silica network.

To produce a mesoporous solid, the surfactant species must be removed, which can be achieved by calcination. Aligned monoliths of the silica-surfactant composite were calcined in oxygen to produce oriented mesoporous silica (*29*). The resulting samples were white and retained their original bulk shape and form. During calcination, the mesoscale periodicity was also preserved: Although some lattice shrinkage and broadening of the diffraction peaks are observed, the XRD features obtained after calcination (Figs. 2B, 3B, and 4B) are quite similar to those obtained before removal of the surfactant (Figs. 2A, 3A, and 4A). The pattern of pairs of arcs oriented along a single axis is clearly observed.

For the calcined mesoporous silica, integration of 30° slices around the radial angle χ in the area of intense scattering intensity (Fig. 3B, solid line) again shows (100), (110), and (200) diffraction peaks, corresponding to the hexagonal MCM-41 structure. Comparison of the on-axis (solid line) versus off-axis (dashed line) integrations indicates furthermore that about 72% of the calcined sample is oriented (*28*). The hexagonal mesostructure observed in XRD was also seen in transmission electron micrographs, where well-defined lattice planes and sharp electron diffraction patterns were found. Integration over the $(100)_{hex}$ diffraction peak around χ indicates a moderately Gaussian distribution of pore orientations with a FWHM of 53° (Fig. 4B). The FWHM of the orientation distribution and the percentage of oriented domains are almost identical on going from the oriented liquid crystal precursor (55 ± 5°, 80%) to the polymerized silica-surfactant composite (49°, 78%) and to the final calcined mesoporous silica product (53°, 72%). These results demonstrate the robustness of the macroscopic alignment introduced by the liquid crystal processing procedure.

Nitrogen adsorption-desorption measurements (Fig. 5) and analyses establish that the aligned calcined material is mesoporous with a high internal surface area and a narrow pore-size distribution (*30*)). Data were collected on an aligned calcined sample prepared as described above (method 1), with synthesis conditions and procedures that were identical to those associated with Figs. 1 to 4. A pore-size distribution centered at 22 Å (FWHM = 4 Å) was obtained (*30*), consistent with the $d_{(100)}$ spacing of 30 Å measured from the XRD patterns in Fig. 3 and a silica wall thickness of 10 to 15 Å (*31*). The Brunauer-Emmett-Teller (BET) surface area and single-point pore volume were 1500 m^2/g and 1.1 cm^3/g, respectively (*30*), which are near the high end of values reported for mesoporous silicates in this size regime [$d_{(100)}$ = 30 Å] (*1*, *8*). This combination of high surface area and high pore volume may be due in part to a more uniform distribution of silicate anions in the equilibrium silicate-surfactant liquid crystal precursor phases be-

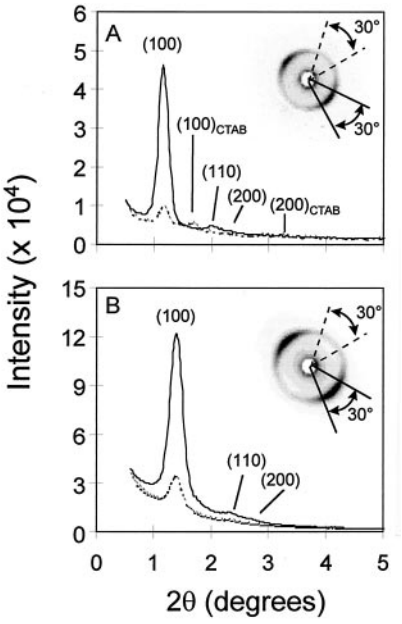

Fig. 3. Integrated XRD data plotted as intensity versus 2θ for (**A**) the aligned polymerized hexagonal silica-surfactant mesophase composite and (**B**) the aligned calcined hexagonal mesoporous silica. The solid lines were generated from integrations over 30° slices centered on the most intense regions of the diffraction patterns shown in Fig. 2; the dashed lines were generated from 30° integrations centered on the perpendicular axes (insets). In (A), the solid line represents scattering from oriented *p6mm* hexagonal silica-surfactant domains, whereas the dashed line corresponds to scattering intensity from unaligned *p6mm* hexagonal domains. Some scattering from monoclinic crystalline CTAB can also be faintly observed [$d_{(100)}$ = 26 Å (*40*)]. The same features are observed in (B) for the oriented hexagonal mesoporous silica sample after calcination, a process that removes all of the surfactant species, including the crystalline CTAB.

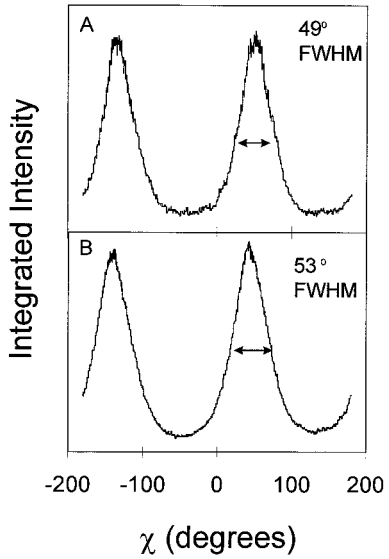

Fig. 4. Radial integrations over the width of the $(100)_{hex}$ diffraction peak (in Fig. 2) plotted as integrated x-ray scattering intensity versus radial position χ for (**A**) the aligned polymerized hexagonal silica-surfactant composite and (**B**) aligned calcined hexagonal mesoporous silica. The data show Gaussian distributions of domain orientations with a 49° FWHM for the aligned silica-surfactant composite in (A) and a 53° FWHM for the aligned calcined mesoporous material in (B).

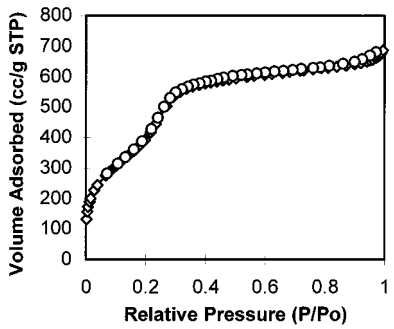

Fig. 5. Nitrogen adsorption isotherm data obtained on aligned calcined mesoporous silica synthesized through a liquid crystalline intermediate and polymerized with vapor phase HCl (method 1). The nitrogen adsorption and desorption isotherms are characteristic of mesoporous samples (*41*).

fore polymerization of the silicate species. This is expected to lead to more homogeneous incorporation of silica into the periodic mesostructures, contributing perhaps to a more uniform overall pore structure.

Liquid crystalline processing, followed by inorganic (or organic) polymerization offers a wide range of possibilities for the formation of hierarchically structured materials. Alignment of anisotropic liquid crystalline materials can be induced by the application of a variety of external fields, including shear fields (*32*), electric fields (*33*, *34*), and magnetic fields (*35*), and by direct contact with surfaces (capillary alignment) (*34*). In addition to the magnetic field alignment presented above, we have observed both shear and capillary alignment in our experiments involving silicate-surfactant liquid crystals. In the case of capillary alignment, these experiments show that orientational order is similarly preserved on polymerization of the inorganic component of the silicate-surfactant liquid crystal. Moreover, within the methodology of magnetic field alignment, the resultant orientational ordering can be controlled by the manipulation of the mesophase composition on the basis of the molecular diamagnetic susceptibilities of the constituent species (*24*). For example, depending on the choices of surfactant and cosolvent molecules, hexagonal composites can be oriented such that the domain axes are aligned either parallel to the applied field or perpendicular to it; similar results can be obtained for lamellar phases (*24*).

The fact that these oriented materials are prepared with a liquid crystalline intermediate offers flexibility in controlling the shape of the composite or mesoporous solid products. As discussed above, the silicate-surfactant liquid crystals used in these experiments are viscoelastic and thus retain orientational alignment on time scales of months or longer. When the materials are heated above their anisotropic-to-isotropic transition temperature, however, their viscoelasticity is substantially reduced, and they can thus be processed into bulk structures and films with different macroscopic shapes by selection of the desired size and form of the reaction vessel.

Important possibilities also exist for mesostructural variability in these systems. For example, under alkaline conditions, the pore size can be controlled over a wide range (20 to 150 Å) by variations in the surfactant chain length and the quantity of the cosolvent (*1*). Such strategies can also be applied to oriented samples. Besides the *p6mm* hexagonal phase, examples of other potentially alignable silicate-surfactant structures include the 1D lamellar phase (*24*), the 2D centered rectangular *cmm* phase (*36*), and the 3D hexagonal phase $P6_3/mmc$ (*37*). More generally, any inorganic-organic composite with a noncubic structure that can be produced through a liquid crystalline intermediate should be alignable through appropriate choices of composition, temperature, and applied field. Examples of such systems include hexagonal silicate-surfactant composites formed with nonionic ethyleneoxide surfactants that are thought to proceed through a liquid crystalline intermediate (*38*), hexagonal niobium oxide-surfactant composites formed from a liquid crystalline precursor alkyl-NH_2-Nb-$(OEt)_5$ (Et, ethyl) (*3*), and hexagonal CdS-surfactant composites formed by polymerization of a Cd^{2+}-surfactant liquid crystal with H_2S gas (*9*).

The ability to macroscopically orient inorganic-organic mesostructured materials offers a route for controlling the structure of composite solids on multiple length scales. Moreover, it opens the possibility of exploiting the mesoscopic organization of composites or mesoporous solids for applications in which ordered, anisotropic, monolithic structures are required. Promising applications include separations, catalysis, chemical sensors, and host-guest chemistry. Processing silicate-surfactant mesophases by established liquid crystal methods and then polymerizing the inorganic component provide a wide range of opportunities for producing ordered inorganic-organic composites. These composites may be used to prepare high surface area mesoporous materials with tailored properties, including pore orientation, mesoscopic periodicity, and macroscopic morphology.

REFERENCES AND NOTES

1. C. T. Kresge, M. E. Leonowitz, W. J. Roth, J. C. Vartuli, J. S. Beck, *Nature* **359**, 710 (1992); J. S. Beck *et al*., *J. Am. Chem. Soc.* **114**, 10834 (1992).
2. A. Firouzi *et al*., *Science* **267**, 1138 (1995).
3. D. M. Antonelli, A. Nakahira, J. Y. Ying, *Inorg. Chem.* **35**, 3126 (1996); D. M. Antonelli and J. Y. Ying, *Chem. Mater.* **8**, 874 (1996); *Angew. Chem. Int. Ed. Eng.* **35**, 426 (1996).
4. T. Abe, A. Taguchi, M. Iwamoto, *Chem. Mater.* **7**, 1429 (1995); J. A. Knowles and M. J. Hudson, *J. Chem. Soc. Chem. Commun.* **1995**, 2083 (1995); D. M. Antonelli and J. Y. Ying, *Angew. Chem. Int. Ed. Eng.* **34**, 2014 (1995); U. Ciesla, S. Schacht, G. D. Stucky, K. K. Unger, F. Schüth, *ibid.* **35**, 541 (1996); Z.-R. Tian *et al.*, *Science* **276**, 926 (1997).
5. G. Fu, C. Fyfe, W. Schwieger, G. T. Kokotailo, *Angew. Chem. Int. Ed. Eng.* **34**, 1499 (1995).
6. P. T. Tanev and T. J. Pinnavaia, *Science* **267**, 865 (1995).
7. P. Y. Feng, Y. Xia, J. L. Feng, X. H. Bu, G. D. Stucky, *Chem. Commun.* **1997**, 949 (1997); D. Y. Zhao, Z. H. Luan, L. Kevan, *ibid.*, p. 1009.
8. Q. Huo, D. I. Margolese, G. D. Stucky, *Chem. Mater.* **8**, 1147 (1996).
9. P. V. Braun, P. Osenar, S. I. Stupp, *Nature* **380**, 325 (1996).
10. S. L. Burkett, S. D. Sims, S. Mann, *Chem. Commun.* **1996**, 1367 (1996).
11. A. Sayari, *Chem. Mater.* **8**, 1840 (1996).
12. T. Bein, *ibid.*, p. 1636.
13. J. Caro *et al.*, *Adv. Mater.* **4**, 273 (1992).
14. G. D. Stucky and J. E. MacDougall, *Science* **247**, 669 (1990).
15. C.-G. Wu and T. Bein, *ibid.* **266**, 1013 (1994); *ibid.* **264**, 1757 (1994).
16. Notable exceptions are the recent syntheses of mesoporous silicas as hard spheres, hollow spheres, sheets, and fibers. Transmission electron microscopy suggests that the pores in the sheets and hollow spheres are perpendicular to the film or sphere surfaces. The pores of the optically transparent fibers are parallel to the fiber axis [S. Schacht, Q. Huo, I. G. Voigt-Martin, G. D. Stucky, F. Schüth, *Science* **273**, 768 (1996); Q. S. Huo, J. L. Feng, F. Schüth, G. D. Stucky, *Chem. Mater.* **9**, 14 (1997); Q. S. Huo *et al*., *Adv. Mater.*, in press].
17. The recent synthesis of a silica-surfactant L_3 sponge phase as a glassy solid provides a 3D, random pore system with uniform pore dimensions [K. M. McGrath, D. M. Dabbs, N. Yao, I. A. Aksay, S. M. Gruner, *Science* **277**, 552 (1997)].
18. H. Yang, A. Kuperman, N. Coombs, S. Mamiche-Afara, G. A. Ozin, *Nature* **379**, 703 (1996); H. Yang, N. Coombs, I. Sakolov, G. A. Ozin, *ibid.* **381**, 589 (1996).
19. I. A. Aksay *et al*., *Science* **273**, 892 (1996).
20. S. H. Tolbert, T. E. Schäffer, J. Feng, P. K. Hansma, G. D. Stucky, *Chem. Mater.*, in press.
21. R. Ganguli *et al*., *Nature* **389**, 364 (1997).
22. A. Monnier *et al*., *Science* **261**, 1299 (1993).
23. A. Firouzi, F. Atef, A. G. Oertli, G. D. Stucky, B. F. Chmelka, *J. Am. Chem. Soc.* **119**, 3596 (1997); A. Firouzi, G. D. Stucky, B. F. Chmelka, in *Synthesis of Microporous Materials*, M. L. Occelli and H. Kessler, Eds. (Dekker, New York, 1996), pp. 379–389.
24. A. Firouzi, D. J. Schaefer, S. H. Tolbert, G. D. Stucky, B. F. Chmelka, *J. Am. Chem. Soc.* **119**, 9466 (1997).
25. The ^2H NMR measurements were acquired at 11.7 T on a Chemagnetics (Fort Collins, CO) CMX-500 spectrometer with the use of a standard quadrupolar-echo pulse sequence with $\pi/2$ pulses of 4 to 6 ms, a 50-ms echo delay, a recycle delay of 0.25 s, and 3600 to 7200 signal acquisitions. We performed simulations of the ^2H NMR line shapes using the measured quadrupolar splitting of each Pake powder pattern as an input parameter and fitting both the fraction of oriented material in the sample and the width of the orientation distribution. A Gaussian distribution of domain directors about the uniaxial orientation direction was assumed (*24*).
26. This degree of alignment can be improved in many cases by slowly temperature cycling the sample through the anisotropic-to-isotropic transition in the presence of the applied magnetic field. In addition, the degree of orientation can be expected to be improved by an increase in the strength of the orienting magnetic field or by changes in the mixture composition, particularly the choice of the surfactant molecules and organic solutes (*24*). For example, recent experiments with the double-headed surfactant (*p*-phenylenedimethylene)bis(hexadecyl-dimethylammonium) dibromide [F. M. Menger and C. A. Littau, *J. Am. Chem. Soc.* **115**, 10083 (1993)], which has a larger absolute molecular diamagnetic susceptibility than CTAB, have shown that a FWHM distribution of only 40° can be achieved with 76% of the hexagonal domains oriented parallel to the applied magnetic field.
27. A related procedure has been used by other researchers [C. A. Fyfe and G. Fu, *J. Am. Chem. Soc.* **117**, 9709 (1995)].
28. Oriented fractions were calculated by comparison of scaled integrated diffraction intensities for the on- and off-axis 30° integrations in Fig. 3. We scaled on-axis integrations by numerically integrating a 30° slice of a 49° (uncalcined) or 53° (calcined) Gaussian (FWHM); we scaled off-axis integrations by using a 30° slice of an isotropic scattering ring.
29. Polymerized samples were heated under flowing N_2 from room temperature to 500°C over 8 hours and subsequently held at 500°C for 6 hours. The gas was then switched to O_2 for 6 hours at 500°C, followed by cooling over 4 hours to room temperature, again under flowing O_2.
30. Samples were analyzed for porosity with nitrogen

adsorption isotherms recorded on a Micromeritics ASAP 2000 porosimeter. Surface areas were determined by the BET method; pore volumes were obtained from single-point measurements at a normalized partial pressure (P/P_o) of 0.9837. Pore-size distributions were determined by the Barrett-Joyner-Halenda (BJH) method. The accuracies of the BJH and BET methods in this small size regime are limited, and, therefore, the resulting pore-size distributions and surface areas should be considered approximate.
31. A $d_{(100)}$ spacing of 30 Å corresponds to a lattice constant a of $2d\sqrt{3}$ or 35 Å.
32. L. Powers and P. S. Pershan, *Biophys. J.* **20**, 137 (1977); L. Powers and N. A. Clark, *Proc. Natl. Acad. Sci. U.S.A.* **72**, 840 (1977); G. G. Barclay, S. G. McNamee, C. K. Ober, K. I. Papathomas, D. W. Wang, *J. Polym. Sci. Part A Polym. Chem.* **30**, 1845 (1992); M. Lukaschek, D. A. Grabowski, C. Schmidt, *Langmuir* **11**, 3590 (1995); J. A. Müller, R. S. Stein, H. H. Winter, *Rheol. Acta* **35**, 160 (1996).
33. P. A. Winsor, in *Liquid Crystals and Plastic Crystals*, G. W. Gray and P. A. Winsor, Eds. (Ellis Harwood, Chichester, UK, 1974), vol. 2, pp. 122–143; K. Amundson, E. Helfand, X. Quan, S. D. Hudson, S. D. Smith, *Macromolecules* **27**, 6559 (1994).
34. A. M. Figueredo Neto and L. Q. Amaral, *Mol. Cryst. Liq. Cryst.* **74**, 109 (1981).
35. H. Gutman, Z. Luz, E. J. Wachtel, R. Poupko, J. Charvolin, *Liq. Cryst.* **7**, 335 (1990); M. Jansson, R. L. Thurmond, T. P. Trouard, M. F. Brown, *Chem. Phys. Lipids* **54**, 157 (1990); H. Gutman, A. Loewenstein, Z. Luz, R. Poupko, H. Zimmermann, *Liq. Cryst.* **9**, 607 (1991); W. Schnepp, S. Disch, C. Schmidt, *ibid.* **14**, 843 (1993).
36. Q. Huo and G. D. Stucky, manuscript in preparation.
37. Q. Huo, R. Leon, P. M. Petroff, G. D. Stucky, *Science* **268**, 1324 (1995).
38. G. S. Attard, J. C. Glyde, C. G. Göltner, *Nature* **378**, 366 (1995).
39. Some cationic surfactant is expelled from the composite as the anionic silica charge density is reduced because of polymerization (*22*). The crystalline CTAB peaks are oriented because the plate-like crystals tend to lie flat on the surfaces of the bulk composite.
40. Powder Diffraction File entry 80-1746 (International Center for Diffraction Data, Newtown Square, PA, 1992).
41. P. I. Ravikovitch, S. C. Odomhnaill, A. V. Neimark, F. Schüth, K. K. Unger, *Langmuir* **11**, 4765 (1995).
42. Supported by NSF grants CHE-9626523 (S.H.T.), DMR-9520971 (G.D.S.), and DMR-9257064 (B.F.C.); the U.S. Army Research Office (DAAH04-96-1-0443); a Henkel Foundation–American Chemical Society Research Fellowship in Colloid and Surface Chemistry (A.F.); the David and Lucile Packard Foundation (B.F.C.); and Shell Research B.V. (B.F.C.). This work made use of instrumentation supported in part by the NSF Division of Materials Research under grant DMR-922257 and through the University of California, Santa Barbara, Materials Research Laboratory under award DMR-9632716. B.F.C. is a Camille and Henry Dreyfus Teacher-Scholar and an Alfred P. Sloan Research Fellow.

3 July 1997; accepted 29 August 1997

The Response of Jupiter's Magnetosphere to an Outburst on Io

Michael E. Brown* and Antonin H. Bouchez

A 6-month-long monitoring campaign of the Io plasma torus and neutral cloud was conducted to determine the characteristics of their interaction. During the observations, a large outburst of material from Io—inferred to be caused by the eruption of a volcanic plume on Io—caused a transient increase in the neutral cloud and plasma torus masses. The response of the plasma torus to this outburst shows that the interaction between Io and Jupiter's magnetosphere is stabilized by a feedback mechanism in which increases in the plasma torus mass cause a nonlinear increase in loss from the plasma torus, limiting plasma buildup.

Jupiter's magnetosphere is filled with plasma mostly derived from Io, the innermost of the large satellites of Jupiter and the most volcanically active body in the solar system. The magnetospheric plasma and the volcanos on Io are tightly coupled: the volcanos feed material, primarily S and O, to the atmosphere and surface frosts of Io (*1*); bombardment by magnetospheric plasma removes the atmosphere and frosts into an extended cloud of gas surrounding the satellite's orbit (*2*). This gas is ionized by collisions with the magnetospheric plasma, becomes incorporated into the Io plasma torus (the inner, dense portion of the jovian magnetosphere), and returns to further bombard Io.

The plasma density in the Io plasma torus remained roughly constant over at least a 13-year period (*3*), even though volcanic activity on Io is presumably sporadic (*4*). The stability of the system in the face of variable volcanic input must be achieved through some feedback mechanism, either through the regulation of supply to the extended gas cloud surrounding Io ("supply-limited") or through regulation of loss from the plasma torus ("loss-limited") (*5, 6*).

The system will be supply-limited if an increase in the plasma bombardment rate causes a less strong increase in the rate of supply to the extended neutral gas cloud. Two atmospheric models that lead to supply-limitation include an ionospheric buffering model, where an increase in plasma bombardment increases Io's ionosphere, which then begins to deflect the plasma bombardment, thus reducing the supply of material to the neutral cloud (*7*), and a constant-source model, where supply to the neutral cloud is a characteristic solely of Io's atmosphere and does not change with changing plasma bombardment (*8*).

The system will be loss-limited if increases in plasma mass cause even larger increases in plasma loss. One loss-limited plasma transport model suggests that depletion of the plasma torus is driven by nonlinear centrifugally driven diffusion caused by the fast rotation of the jovian magnetosphere. In such a system, the diffusion rate is proportional to the square of the plasma density (rather than to the first power of the density for linear diffusion) (*9*). Another loss-limiting mechanism could be plasma transport initiated by large-scale plasma instability (*10*), where the onset and growth of the instability would lead to a nonlinear plasma loss.

To determine the type of feedback mechanism operating on Io (Fig. 1), we monitored emission from the Io plasma torus and the extended neutral cloud of material surrounding Io's orbit for 6 months. We report a major perturbation to the system that occurred in March 1992, most likely as a result of a volcanic outburst on Io.

We observed S^+ in the Io plasma torus and Na in the extended neutral cloud on 56 clear nights between 1 December 1991 and 1 June 1992, using the Lick Observatory 0.6-m coudé auxiliary telescope connected to the Hamilton echelle spectrograph (*11*). These two species were chosen because they have the brightest emission intensities in the visible wavelength range for a plasma torus ion (S^+) and neutral cloud atom (Na). About 10% of the plasma torus at a distance of 6 R_J is composed of S^+ (*12*). Sodium is about 100 times less abundant than S or O in the neutral cloud (*2*), but we will attempt to use it as a tracer of the major species. From these spectra, we extract emission intensity as a function of distance from Jupiter along the entire slit and compare the behavior of S^+ from the plasma torus and Na from the neutral cloud (Fig. 2) (*13*).

A sudden increase in the brightness (and thus, mass) of the neutral Na cloud started around Julian date 2448680, or 27 February 1992 (hereafter, only the last three digits of each Julian date will be given), followed by a more gradual increase in the plasma torus emission intensity. The Na cloud mass increased by an average of about a factor of 2 for at least 65 days, with transient increases of higher than a factor of 4. The S^+ plasma

Division of Geological and Planetary Sciences, California Institute of Technology, Pasadena, California 91125, USA.

*To whom correspondence should be addressed. E-mail: mbrown@gps.caltech.edu

Magnetic Field Alignment of Ordered Silicate-Surfactant Composites and Mesoporous Silica

Sarah H. Tolbert *et al.*

Science **278**, 264 (1997);
DOI: 10.1126/science.278.5336.264